International Journal of Research in Engineering, Science and Management
Volume 4, Issue 11, November 2021
https://www.ijresm.com | ISSN (Online): 2581-5792

One Indoor Channel Model per Cluster for MIMO Systems Polarized

Ahmed Alzahmi*
Department of Electrical Engineering, Faculty of Engineering, University of Tabuk, Tabuk, Saudi Arabia

***Abstract*: A cluster channel model for an indoor environment, which includes the characterization of polarization, is presented in this work. A measurement campaign was carried out in an indoor environment at 3.6 GHz, with a bipolarized transmitter and a 3-pole receiver. The rays are detected with the SAGE algorithm, and cross-polar discrimination (XPD) per ray is defined. Clusters are identified in the azimuth - elevation - delay domains, with an automatic clustering algorithm. The properties of the clusters are investigated and polarization characteristics by cluster are extracted. The obtained model is simulated, and the independent parameters are compared with the measurements for validation. The results indicated that the XPDs of the rays have a lognormal distribution per cluster.**

***Keywords*: MIMO, polarization, SAGE, cluster.**

1. Introduction

Polarization diversity has been proposed as a solution to reduce the size of multi-antenna terminals (MIMO). By using antennas, co-located, perpendicularly polarized, it is possible to reduce the inter-antenna correlation while keeping the size of the equipment reasonable [1]-[5]. Several geometric models have recently been developed to describe the behavior of the wireless communications channel (COST273, 3GPP / 3GPP2, etc.). Most of these models describe the channel as a sum of rays, which are grouped into clusters [6-8]. In this case, a cluster is defined as a group of rays with identical propagation characteristics. Numerous articles have investigated the polarization properties of geometric models. It is relatively simple to introduce polarization into a geometric model by considering the polarization of each ray. The global polarization mechanisms are implicitly recreated via summing all the rays at the emitter and the receiver [9]-[11]. An outdoor measurement campaign was carried out and the polarization characteristics of the rays are investigated [9]. The polarization is defined by cluster, and the properties of these clusters are presented [12]. This article aims to examine the properties of cluster polarization in an indoor environment. The rays are detected with a high-resolution algorithm and are grouped into clusters with an automatic clustering algorithm. The characteristics of the clusters are then extracted from the measurements. The article includes experimental setup, data processing, and automatic clustering. The properties of these clusters are also extracted and presented, and a comparison between the simulated model and the measurements is introduced for validation.

2. Experimental Setup and Data Extraction

A. Experimental Apparatus

The measurement campaign was carried out in an indoor office environment, illustrated in Fig. 1. The rooms contain furniture and equipment, the walls are made of concrete and panels, and there are windows along with the lab and offices. Measures have been taken to 16 different locations in the laboratory and the offices. The transmitter and the receiver were never in direct line of sight.

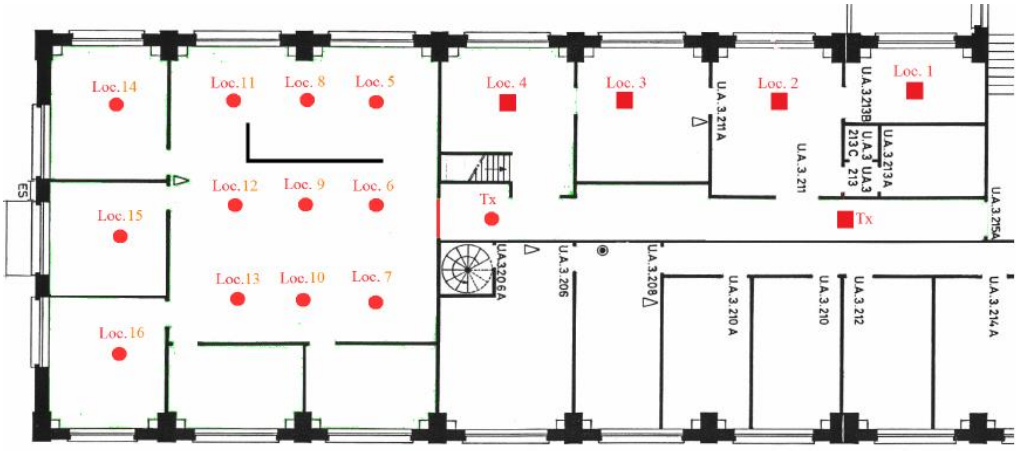

Fig. 1. Map of the measurement environment

*Corresponding author: ahmed.alzahmi@yahoo.com

$$\begin{bmatrix} S_{H1V}(f) & S_{H1H}(f) \\ S_{H2V}(f) & S_{H2H}(f) \\ S_{VV}(f) & S_{VH}(f) \end{bmatrix}_{n,l} = \begin{bmatrix} f_{\theta H1}(\theta_l, \emptyset_l) & f_{\emptyset H1}(\theta_l, \emptyset_l) \\ f_{\theta H2}(\theta_l, \emptyset_l) & f_{\emptyset H2}(\theta_l, \emptyset_1) \\ f_{\theta V}(\theta_l, \emptyset_l) & f_{\emptyset V}(\theta_l, \emptyset_l) \end{bmatrix} \begin{bmatrix} \alpha_{\theta V} & \alpha_{\emptyset H} \\ \alpha_{\emptyset V} & \alpha_{\emptyset H} \end{bmatrix}_l e^{-j2\pi\tau_l f} e^{j\frac{2\pi}{\lambda} r_n \cdot u_r(\theta_1, \emptyset_1)} \quad (1)$$

At each location, a Uniform Cubic Virtual Antenna Array (RVCU) was achieved by adjusting the receiving antenna location using an automatic positioner. All elements of the virtual network were separated by half-wavelength. The receiving antenna was a tripole, consisting of three short antennas polarized perpendicularly. The transmitter was a log-periodic antenna with an angular aperture of 70 °. Anechoic panels were placed behind the transmitter to minimize the effects of side lobes. At each position of the RVCU, the frequency responses of the three receiving antennas were measured simultaneously with a Rhode & Schwarz ZVA-24 vector network analyzer. After measuring all the RVCU for one emitter polarization, the polarization of the emitter was changed to virtually create a bipolarized emitter. The central working frequency was 3.6 GHz with a 200 MHz band. All measurements were made at night, so the environment can be considered perfectly static between the two measurements. Further details about the experimental setup are discussed in [13].

B. Data Analysis and Ray Extraction

The measurements were processed to find the directions of arrival of the different rays at the receiver. A slightly modified version of the SAGE algorithm, Space Alternating Generalized Expectation-Maximization, was utilized to detect the directions of ray arrival [14], thus as the power of each combination of transceiver polarizations. The modification of the SAGE algorithm can spot all three polarizations at the receiver. The signal model that has been used for SAGE is as follows: for a three-pole receiving antenna network and a transmitter bipolarized, the contribution to the frequency response of the lth ray to the nth element of the lattice is given by (1).

In equation (1), S_{XY}: is the signal received on the antenna with X polarization for a transmitter with Y polarization, V, H, H_1, H_2, respectively: the vertical emitting/receiving polarization, the horizontal emitting polarization, first horizontal receiving polarization, second horizontal receiving polarization, $f_{\theta X}$: component θ of the antenna radiation pattern with receiving X polarization, $f_{\varphi X}$: component φ of the antenna radiation pattern with receiving polarization X, τ_l, θ_l, φ_l: respectively the delay, the co-elevation and the azimuth of radius l, $\alpha_{\theta X}$: amplitude of the component θ of the ray with emitting polarization X, $\alpha_{\varphi X}$: amplitude of the component φ of the ray with emitting polarization X, λ: wavelength, r_n: position vector of the element *n* of the network, $u_r(\theta_l, \varphi_l)$: unit vector pointing in the direction (θ_l, φ_l).

As the radiation patterns of the transmitting antennas are not included in (1), the terms $\alpha_{\theta X}$ and $\alpha_{\varphi X}$ comprise the effects of transmitting antennas. For the SAGE algorithm to provide reliable results, precise antenna and network calibration are required. In particular, due to implementing a virtual network, there is no coupling problem of antennas, and the theoretical expression of network gain can be used. Fig. 2 shows the diagrams of radiation from the receiving antennas that were measured in an anechoic chamber. For each measurement location, 100 rays were detected with the algorithm WISE. An instance of the detected rays is given in Fig. 3. For each ray, the delay, the co-elevation, azimuth, and the α polarization matrix were perceived. Only the rays that had a power 10 dB higher than the noise threshold were selected for further processing. Nota that part of the power was not considered during rays detection with high algorithms resolution. That power "Residual", shown in Fig. 4, is often called the diffuse power [15]. The analysis which follows focuses on coherent rays and does not model this diffuse component.

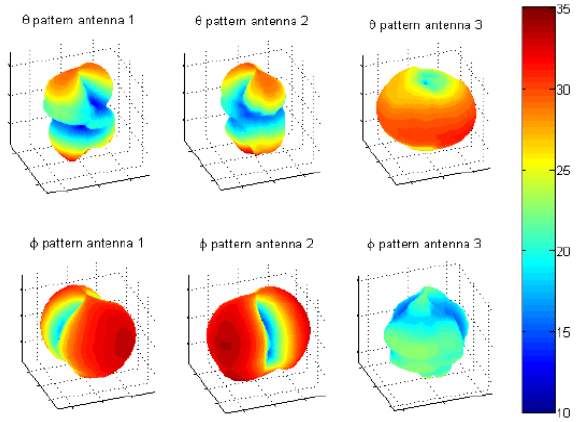

Fig. 2. Components θ and φ of the radiation patterns of the 3 antennas of the receiving tripole

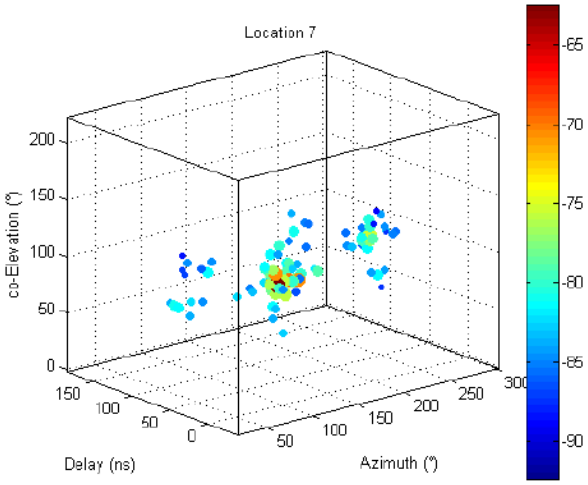

Fig. 3. Rays detected with SAGE in the azimuth - co-elevation - delay domains

C. Identification of Clusters

The problem of ray clustering is an issue that has received a lot of attention recently. Visual clustering has been used for some time, but since visual inspection of data contains a rate of subjectivity, it is difficult to interpret and compare results. Several automatic clustering techniques have been proposed, including algorithms hierarchical clustering [16], Gaussian clustering [17], and the K-power means algorithm [16], [18].

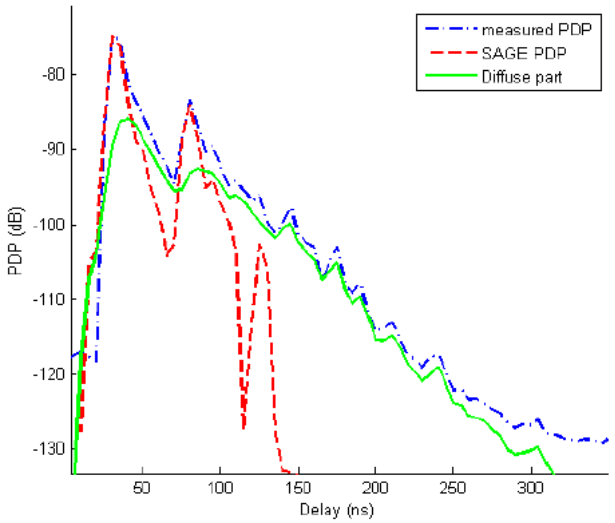

Fig. 4. Measured PDP, reconstructed PDP with SAGE and diffused power

Since the definition of a cluster mainly depends on the clustering algorithm used, it is crucial to specify how the cluster is defined. A cluster is described as a group of rays with identical propagation characteristics, which justifies the use of the K-power means algorithm as the recent results of COST 273 [6]. The K-power means that the algorithm will, for a given number of clusters, group the rays to reduce the total sum of the square distances (weighted by their power) of the rays at the centroids of their cluster. Thus, the overall spread of the clusters is minimized. Details on the exact implementation of K-power means can be found in [18]. In the proposed work, the rays are clustered in the azimuth - co-elevation - delay domains.

The second problem with automatic clustering algorithms is determining the number of exact clusters. As mentioned above, the K-power means that the algorithm will minimize the spreading global number of clusters yet will not give any information on the exact number of clusters. It exists several indices to determine the optimal number of clusters, the most popular method is by Davies - Bouldin [19]. This index is a measure of the ratio between the overall intra-cluster spread and the minimum inter-cluster distance. The minimum of this index, therefore, provides the optimal number of clusters. This definition also fits well with the proposed work of what a cluster should be. Unfortunately, due to the difference in scale between the global intra-cluster sprawl and the minimum inter-cluster distance, this index tends to increase or decrease monotonically depending on the number of clusters. To avoid this trend, a standardized version of the index Davies - Bouldin was used: the Kim - Parks index [20]. This index normalizes the intra-cluster sprawl overall and the minimum inter-cluster distance from their obtained values for the minimum and the maximum number of clusters. Fig. 5 shows an example of the evolution of the index of Kim - Parks for several clusters ranging from 2 to 10. Note that with 4 clusters, the index decreases significantly. For all measurements, a clear minimum is observed to determine the optimal number of clusters.

This automatic clustering algorithm was applied for all measurement locations. Fig. 6 shows an example of ray clustering. In most cases, between 4 and 6 clusters have been identified. Clusters with a powerless than 1% of the total power of the location of measurements were discarded from the dataset.

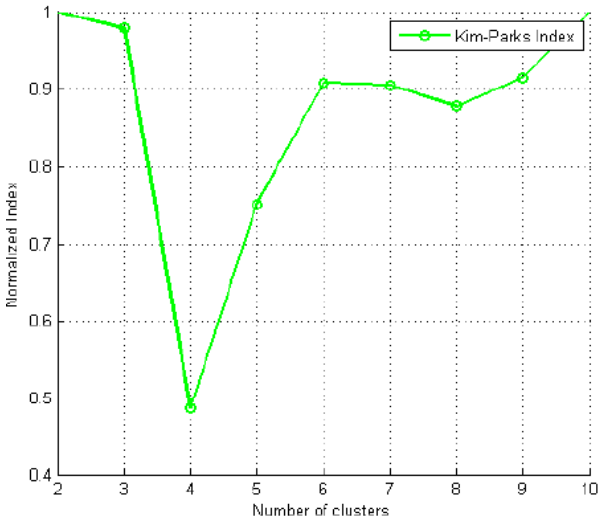

Fig. 5. Evolution of the Kim - Parks index for several clusters ranging from 2 to 10

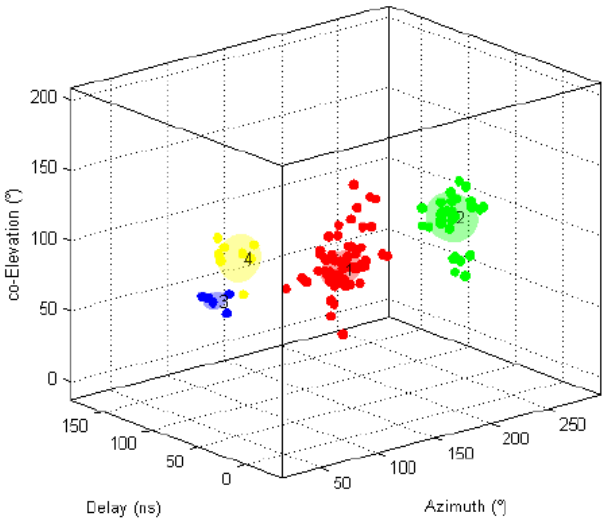

Fig. 6. Clustering of rays into 4 clusters

3. Experimental Results

The polarization characteristics of each ray are fully defined by the three following cross-polar discrimination values:

$$XPD_{V,l} = \frac{|\alpha_{\theta V,l}|^2}{|\alpha_{\phi V,l}|^2} \quad (2)$$

$$XPD_{H,l} = \frac{|\alpha_{\phi H,l}|^2}{|\alpha_{\theta H,l}|^2} \quad (3)$$

$$CPR_l = \frac{|\alpha_{\theta V,l}|^2}{|\alpha_{\phi H,l}|^2} \quad (4)$$

After identifying the different clusters, the number of clusters per measurement location can be characterized and each cluster

k is described by a certain number of parameters: the average angles of arrival of the clusters φ_k and θ_k, cluster delay τ_k, cluster delay spread $\sigma_{\tau k}$, cluster angular spreads $\sigma_{\varphi,\,k}$ and $\sigma_{\theta,\,k}$ and cluster power γ^2_k. The polarization characteristics of the cluster are described by the mean and the standard deviation of the XPDs of the different radii of the cluster: $\mu(XPD_{V,k})$, $\sigma(XPD_{V,k})$, $\mu(XPD_{V,\,H})$, $\sigma(XPD_{V,\,H})$, $\mu(CPR_k)$ and $\sigma(CPR_k)$. Table 1 shows the measured values for the parameters of the clusters.

The power of the cluster is defined by,

$$\gamma_k^2 = \sum_{i,j} \left|\alpha_{i,j}\right|^2$$

The arrival azimuth φ_k, the delay τ_k and the power γ^2_k of each cluster are normalized concerning φ_0, τ_0 and γ^2_0 of the most powerful cluster. This means that for each measurement location, the most powerful C_0 cluster is such that $\varphi_0 = 0°$, $\tau_0 =$ 0 ns and $\gamma^2_0 = 0$ dB. The different parameters of the clusters were extracted from the measurements, and the properties have been observed. First, the distribution of the number of clusters by measurement location is described by a minimum of 3 plus a random variable with a distribution of Fish.

The mean of the Poisson distribution is $\overline{n_e} = 1.69$. Second, the azimuth kφ and the delay k τ of all clusters (except the most powerful clusters) compared to the most powerful clusters are described by 3 percentiles (10%, 50%, and 90%) which are determined from the measurements. Third, the co-elevation θ_k of the clusters is defined by 3 percentiles (10%, 50%, and 90%) which are determined from the measurements. Next, the spreads $\sigma_{\tau,\,k}$, $\sigma_{\varphi,\,k}$ and $\sigma_{\theta,\,k}$ have a lognormal distribution, with values ranging from 2 to 15 ns for $\sigma_{\tau,\,k}$, de 5 to 20° for $\sigma_{\varphi,\,k}$ and from 5 to 15° for $\sigma_{\theta,\,k}$. Fifth, the power of clusters decreases with the delay exponentially. The power of clusters has a

Table 1
Measured values for the parameters of the clusters

Cluster parameter	Mean	Standard deviation	10%	50%	90%
ϕ_k [°]	-	-	63.22	221.48	346.45
$Log(\sigma_{\phi,k})$[log(ns)]	2.19	0.82	-	-	-
θ_k[°]	-	-	88.00	92.11	97.00
$Log(\sigma_{\theta,k})$[log(ns)]	2.04	0.41	-	-	-
τ_k [ns]	-	-	-5.55	9.73	44.06
$\sigma_{\tau,\,k}$	1.4	0.59	-	-	-
γ^2_k	-12- (0.06×τ [ns])	5.10	-	-	-
$\mu(XPD_{V,k})$	6.98	4.88	-	-	-
$\sigma(XPD_{V,k})$	8.20	2.97	-	-	-
$\mu\ (XPD_{H,k})$	0.77	4.09	-	-	-
$\sigma\ (XPD_{H,k})$	5.93	2.46	-	-	-
$\mu\ (CPR_k)$	-2.80	5.39	-	-	-
$\sigma\ (CPR_k)$	8.89	2.48	-	-	-

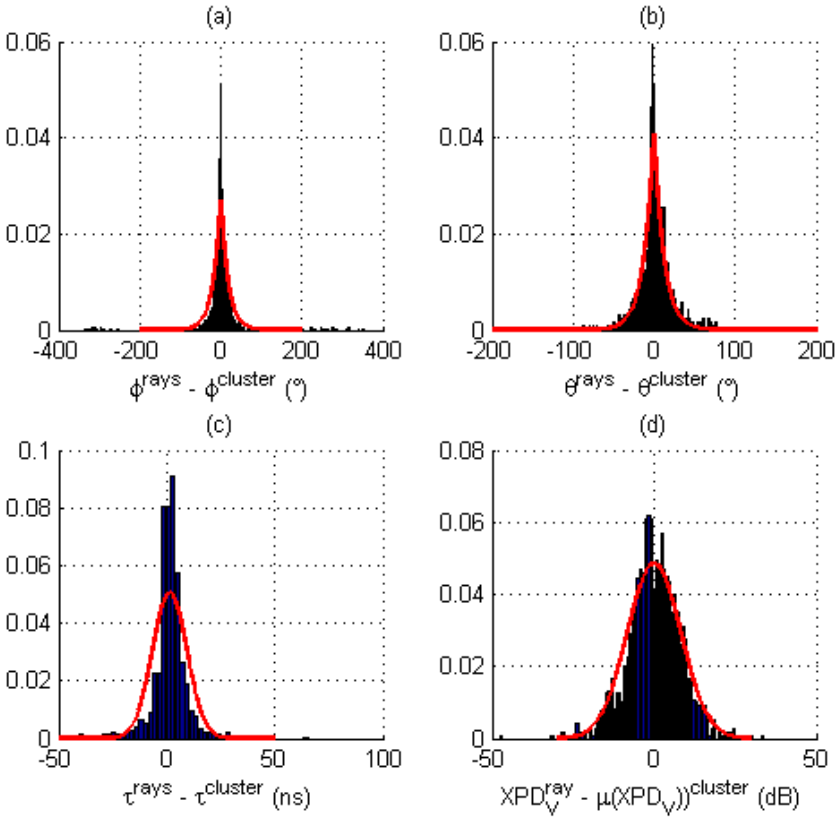

Fig. 7. Distribution of rays inside the clusters

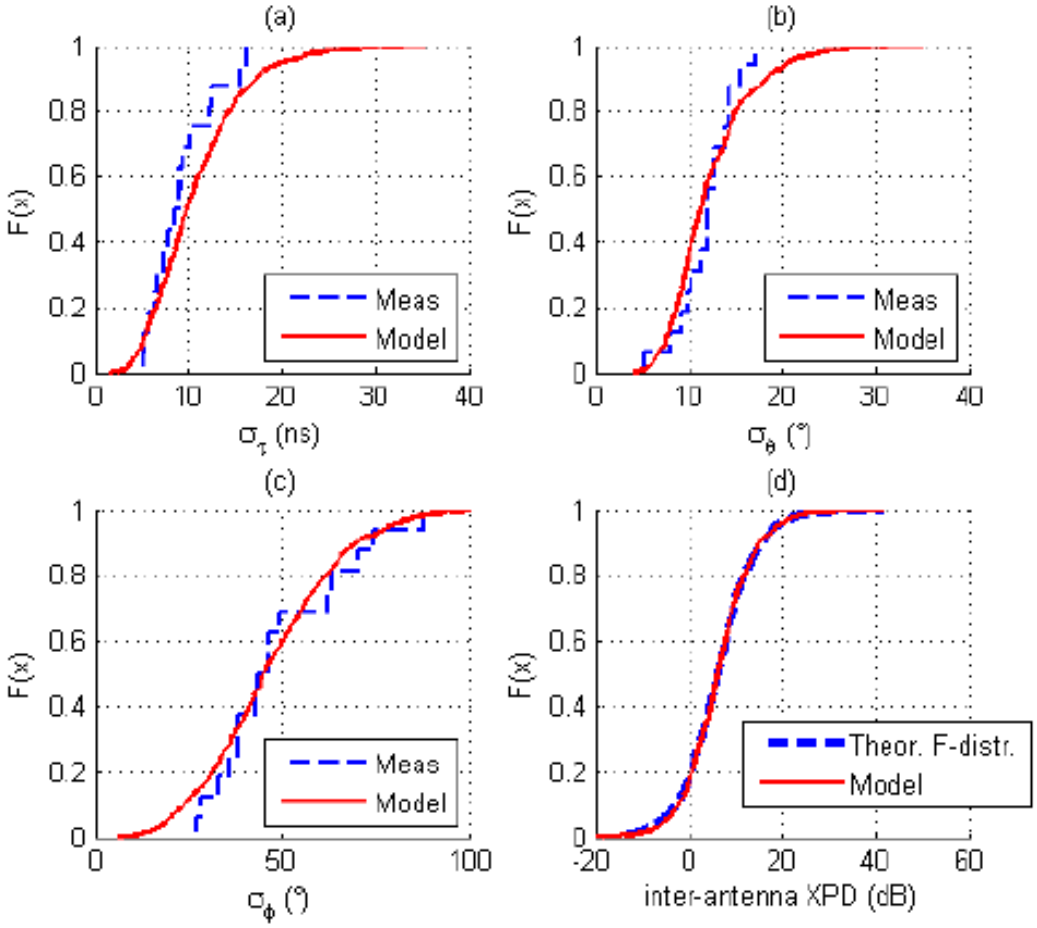

Fig. 8. Comparison between the measurements and the simulated model for (a) the spread of delays (b) the spread of the co-elevations (c) the spread of the azimuths (d) Comparison between the theoretical model in F and the simulated inter-antenna XPD

lognormal distribution around this average decrease. Last, the different means and standard deviations of XPDs have a lognormal distribution. Note that μ ($XPD_{V,H}$) is less than μ ($XPD_{V,k}$) due to cross-polar ratios are defined in spherical coordinates at the receiver. A vertical transmitter emits only waves polarized along θ, while a horizontal transmitter will emit waves that have a φ component but also a component θ in some directions, as shown in Fig. 2. The μ ($XPD_{H,k}$) is therefore already reduced on the side of the issuer.

The radii distributions within the clusters were also examined, with the following conclusions; the angular dispersion of rays in clusters have a Laplace distribution, shown in Fig. 7 (a-b); the dispersion of delays within clusters is approximated by a distribution normal, shown in Fig. 7 (c); the XPDs of the rays have a lognormal distribution inside the clusters with distribution parameters given by μ(XPD_k) and σ(XPD_k). Fig. 7 (d) illustrates the distribution of XPD_V within clusters.

4. Model Validation

The final step is the validation of the model presented by comparing the parameters of the model simulated with measured parameters. It is necessary to choose comparison parameters that were not used to build the model. The spread of delays, the spread of the co elevations, and the spread of the total azimuth (and not by cluster) of the measurements were compared with those of the simulated model in Fig. 8 (a-c). These metrics were not used to build the model and can therefore be considered relatively independent. It can be seen that the delay averaging is significantly overestimated. A better description of the distribution of ray delays in a cluster could further improve this comparison. The spread of co-elevations is slightly overestimated, and the spread of simulated azimuths corresponds well to that measured. Finally, the polarization characteristics are compared. It has been shown in [21] that the local variations of the inter-antenna XPD have an F distribution doubly non-centered. This is also the case in the proposed model, shown in Fig. 8 (d). The agreement between the inter-antenna XPD distribution and the theoretical F model is perfect.

5. Conclusion

In the proposed work, experimental results for the characterization of a MIMO model, polarized and by cluster, were presented. The SAGE algorithm was utilized to detect rays, and the K-power means algorithm was applied to group the rays into clusters. The settings of the clusters were extracted, and ray polarization was defined. The results indicated that ray XPDs have a lognormal distribution per cluster. The simulated model is compared with measurements by independent metrics, and a satisfactory agreement is obtained between the metrics and the simulated model. The polarization behavior of the simulated model obeys the theoretical F distribution.

References

[1] R. Vaughan, "Polarization diversity in mobile communications," in *IEEE Trans. Veh. Technol.*, vol. 39, no. 3, pp. 177–186, 1990.

[2] B. Lindmark and M. Nilsson, "On the available diversity gain from different dual-polarized antennas," in *IEEE J. Select. Areas Commun.*, vol. 19, no. 2, pp. 287–294, 2001.

[3] P. Kyritsi, D. Cox, R. Valenzuela, and P. Wolniansky, "Effect of antenna polarization on the capacity of a multiple element systems in an indoor environment," in *IEEE J. Select. Areas Commun.*, vol. 20, no. 6, pp. 1227–1239, 2002.

[4] V. Erceg, P. Soma, D. Baum, and S. Catreux, "Multiple-input multiple-output fixed wireless radio channel measurements and modeling using dual-polarized antennas at 2.5 ghz," in *EEE Trans. Wireless Commun.*, vol. 3, pp. 2288–2298, 2004.

[5] C. Oestges and B. Clerckx, "MIMO Wireless Communications: From Real-World Propagation to Space-Time Code Design." Oxford, UK: Academic Press (Elsevier), 2007.

[6] L. Correia, "Mobile Broadband Multimedia Networks: Techniques, Models and Tools for 4G." Academic Press, 2006.

[7] G. Calcev, D. Chizhik, B. G¨oransson, S. Howard, H. Huang, A. Kogiantis, A. Molisch, A. Moustakas, D. Reed, and H. Xu, "A wideband spatial channel model for system-wide simulations," in *IEEE Trans. Veh. Technol.*, vol. 56, pp. 389–403, 2007.

[8] N. Czink and C. Oestges, "The COST 273 channel model: Three kinds of clusters," in *Proc. ISSSTA 2008 – International Symposium on Spread Spectrum Techniques and Applications*, 2008.

[9] M. Landmann, K. Sivasondhivat, J. Takada, I. Ida, and R. Thomä, "Polarization behavior of discrete multipath and diffuse scattering in rban environments at 4.5 GHz," in *EURASIP Journal on Wireless Communications and Networking*, 2007.

[10] K. Kalliola, H. Laitinen, L. Vaskelainen, and P. Vainikainen, "Real-time 3D spatial-temporal dual-polarized measurements of wideband radio channel at mobile station," in *IEEE Trans. Instrum. Meas.*, vol. 49, no.2, pp. 439–448, 2000.

[11] T. Kaiser, A. Bourdoux, H. Boche, J. Fonollosa, J. Andersen, and W. Utschick, "Smart Antennas - State of the art", Hindawi, New York, NY, USA, Ed. EURASIP Book Series on Signal Processing and Communications, 2005.

[12] L. Materum, J. Takada, I. Ida, and Y. Oishi, "Mobile Station Spatio-Temporal Multipath Clustering of an Estimated Wideband MIMO Double-Directional Channel of a Small Urban 4.5 GHz Macrocell," in *EURASIP Journal on Wireless Communications and Networking*, Special Issue on APMWS, 2009.

[13] F. Quitin, C. Oestges, F. Horlin, and P. D. Doncker, "Directional Measurements for Indoor Polarized MIMO Systems.," submitted to Transactions on Wireless Communications, 2009.

[14] X. Yin, B. Fleury, P. Jourdan, and A. Stucki, "Polarization estimation of individual propagation paths using the SAGE algorithm," in *Proc. of the PIMRC 2003 - Personal, Indoor and Mobile Radio Communications*, 2003.

[15] N. Czink, A. Richter, E. Bonek, J.-P. Nuutinen, and J. Ylitalo, "Including Diffuse Multipath Parameters in MIMO Channel Models," in *Proc. VTC-F 2007 - IEEE Vehicular Technology Conf.* Fall, 2007.

[16] J. Han and M. Kamber, "Data Mining, Concepts, and Techniques." Morgan Kaufmann Publishers, 2001.

[17] D.-C. Park, O.-H. Kwon, and M. Suk, "Clustering of Gaussian probability density functions using centroid neural network," in *IET Elec. Lett.*, vol. 39, Issue 4, pp. 381–382, 2003.

[18] N. Czink, P. Cera, J. Salo, E. Bonek, J.-P. Nuutinen, and J. Ylitalo, "Improving clustering performance by using the multipath component distance," in *IET Elec. Lett.*, vol. 42, no. 1, pp. 44–45, 2006.

[19] U. Maulik and S. Bandyopadhyay, "Performance evaluation of some clustering algorithms and validity indices," in *IEEE Trans. Pattern Anal. Machine Intell.*, vol. 24, no. 12, pp. 1650–1654, 2002.

[20] D.-J. Kim, Y.-W. Park, and D.-C. D.-J. Park, "A Novel Validity Index for Determination of the Optimal Number of Clusters," in *IEICE Trans. Inf. & Syst.*, vol. E84-D, No. 2, pp. 281–285, 2001.

[21] F. Quitin, C. Oestges, F. Horlin, and P. D. Doncker, "Small-Scale Variations of Cross Polar Discrimination in Ricean Fading Channels," in *IET Elec. Lett.*, vol. 45, no. 4, pp. 213–214, 2009.